RSC Advances

This is an *Accepted Manuscript*, which has been through the Royal Society of Chemistry peer review process and has been accepted for publication.
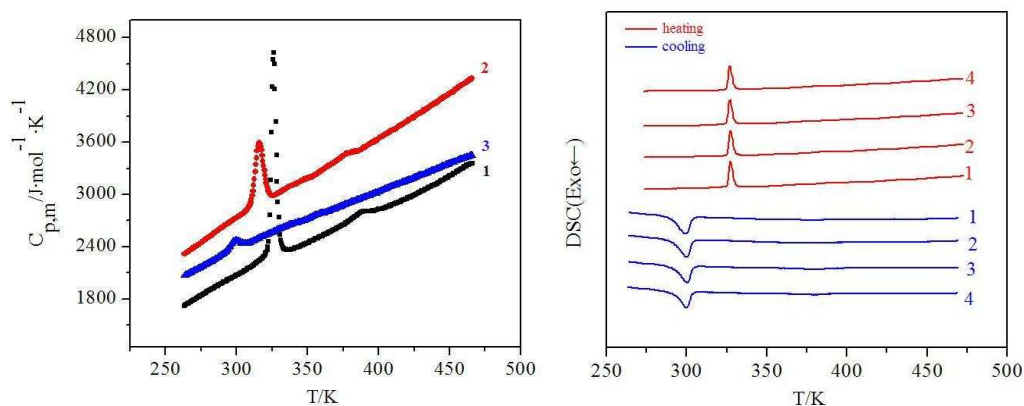
Accepted Manuscripts are published online shortly after acceptance, before technical editing, formatting and proof reading. Using this free service, authors can make their results available to the community, in citable form, before we publish the edited article. This *Accepted Manuscript* will be replaced by the edited, formatted and paginated article as soon as this is available.

You can find more information about *Accepted Manuscripts* in the **Information for Authors**.

ROYAL SOCIETY OF CHEMISTRY

www.rsc.org/advances

Graphical Abstract

Three novel lanthanide complexes [Ln(3,4,5-TEOBA)$_3$phen]$_2$ (Ln=La(1), Pr(2), Eu(3); 3,4,5-TEOBA=3,4,5-Triethoxybenzoate; phen=1,10-phenanthroline) have been synthesized and characterized. Single crystal X-ray diffraction data show the complexes are isostructural. Each complex has two center metals and each center is coordinated by seven oxygen atoms and two nitrogen atoms to form a distorted monocapped square antiprism geometry. Carboxylic group adopts three modes coordinated with center metal: bidentate chelate, bridging bidentate and bridging tridentate. The luminescence of complex 3 shows the characteristic emission of Eu^{3+} ($^5D_0{\rightarrow}^7F_{0-2}$). The thermal decomposition mechanism of title complexes has been studied by TG/DSC-FTIR technology. The heat capacities of complexes 1-3 have been measured by DSC in the temperature range from 263.15 to 463.15 K. In the temperature range of 280 to 350K, there is a solid-to-solid phase transition for each complex, which is further evidenced by four thermal circulating processes with the rate of 10 K/min. Further more, according to the study on the phase transition of four thermal circulating processes under different heating rate, the activation energy (E) and the percent conversion (α) exhibit the fine linear relationship. In the heating and cooling runs, supercooling is observed and the enthalpies of endothermic and exothermic behave differently.

Lanthanide Complexes with 3, 4, 5-Triethoxybenzoic acid and 1,10-phenanthroline: Synthesis, Crystal structures, Thermal decomposition mechanism and Phase transformation kinetics

Xiao-Xia Qi[1,2], Ning Ren[3], Su-Ling Xu[4], Jian-Jun Zhang[1,2*], Guang-Cai Zong[1,2], Jie Gao[1,2], Li-Na Geng[2], Shu-Ping Wang[2], Shi-Kao Shi[2]

[1]Testing and Analysis Center, Hebei Normal University, Shijiazhuang 050024 P.R. China.

[2]College of Chemistry& Material Science, Hebei Normal University, Shijiazhuang 050024 P.R. China.

[3]College of Chemical engineering& Material, Handan College, Handan 056005 P. R. China.

[4]Hebei Super Vision & Inspection Institute of Boiler & Pressure Vessel, Shijiazhuang 050061 P. R. China

[*]E-mail address: jjzhang6@126.com

Abstract:

Three novel lanthanide complexes [Ln(3,4,5-TEOBA)$_3$phen]$_2$ (Ln=La(1), Pr(2), Eu(3); 3,4,5-TEOBA=3,4,5-Triethoxybenzoate; phen=1,10-phenanthroline) have been synthesized and characterized. Single crystal X-ray diffraction data show the complexes are isostructural. Each complex has two center metals and each center is coordinated by seven oxygen atoms and two nitrogen atoms to form a distorted monocapped square antiprism geometry. Carboxylic group adopts three modes coordinated with center metal: bidentate chelate, bridging bidentate and bridging tridentate. The luminescence of complex 3 shows the characteristic emission of Eu^{3+} ($^5D_0 \rightarrow {}^7F_{0-2}$). The thermal decomposition mechanism of title complexes has been studied by TG/DSC-FTIR technology. The heat capacities of complexes 1-3 have been measured by DSC in the temperature range from 263.15 to 463.15 K. In the temperature range of 280 to 350K, there is a solid-to-solid phase transition for each complex, which is further evidenced by four thermal circulating processes with the rate of 10 K/min. Further more, according to the study on the phase transition of four thermal circulating processes under different heating rate, the activation energy (E) and the percent conversion (α) exhibit the fine linear relationship. In the heating and cooling runs, supercooling is observed and the enthalpies of endothermic and exothermic behave differently.

1

Introduction

The exploration of lanthanide complexes has attracted many chemists, owing to the extraordinary properties of lanthanide complexes, such as magnetic, [1] thermodynamics [2, 3] and optical properties. [3, 4] Due to the particularity of 4f shell for rare earth element, lanthanide complexes usually possess diversity structures and fascinating coordination geometry. [5-9] Meanwhile, the high and variable coordination numbers require more strict conditions to synthesis. [10, 11] Lanthanide complexes show the superior luminescence properties, particularly the complexes of Eu, Tb, ect. The f-f transition of metal center in near-infrared spectral regions makes lanthanide complexes potentially applicable for lighting, optical storage and sensors. [12-14] Lanthanide complexes are usually thermally stable. [15-17] According to the study on thermodynamics, the service life of material can be predicted.

Aromatic carboxylic acid ligands as linkers exhibit high affinity to lanthanide center, and can construct lanthanide complexes with center metal in multiple coordinated modes. [18-20] In addition, direct excitation of lanthanide metal center is affected by inefficient absorption of f-f transition, so aromatic carboxylic acid and 1, 10-phenanthroline can be chosen as "antenna" to sensitize luminescence of lanthanide. [21-23]

Above on, our team has been occupied in systematic investigation of lanthanide carboxylic complexes, in particular the thermal property of lanthanide complexes. Recently, we have found and reported the solid-to-solid phase transition of lanthanide aromatic carboxylic complexes, which is rarely reported in literature. [24-27] In this paper, we report the synthesis and characterization of three lanthanide complexes $[Ln(3,4,5\text{-}TEOBA)_3phen]_2$ (Ln= La(1), Pr(2), Eu(3); 3,4,5-TEOBA=3,4,5-Triethoxybenzoate; phen=1,10-phenanthroline). Thermal decomposition mechanism of complexes has been studied by TG/DSC-FTIR technology. The heat capacities of complexes were measured by DSC, and four thermal circulating processes were implemented for complexes 1 and 2. In addition, the phase transformation kinetics of thermal circulating processes for complex 1were also studied.

Experimental

Materials and methods

$LnCl_3 \cdot 6H_2O$ were obtained by the reaction of Ln_2O_3 (Ln=La, Pr, Eu, Beijing Lanthanide Innovation Technology Co., Ltd, 99.9％) and hydrochloric acid in aqueous solution, then

evaporating liquid by water bath heating. Other analytically pure chemicals were purchased and used without further purification.

Equipment and Conditions of the Experiment.

Analyses for C, H and N were carried out on a Vario-ELIII elemental analyzer. Metal content was complexometric titrated by EDTA. The measurement of molar conductance was implemented on DDS-307 conductivity meter with DMSO as the solvent. IR spectra were recorded in the range of 4000-400cm^{-1} on a Bruker TENSOR27 spectrometer using KBr medium pellets. ^{1}H and ^{13}C NMR spectra were measured on Brucker ADVANCE Ⅲ 500M HZ-NMR spectrometer at room temperature with DMSO-d$_6$ as the solvent and TMS as an internal standard. Fluorescence spectra were measured on an F-4600 Hitachi Spectrophotometer. The data of single crystal X-ray diffraction were collected on a smart-1000 diffractometer with graphite-monochromatic Cu Kα (λ=1.54178 Å) for complexes 1-2 and Mo Kα (λ=0.71073 Å) for complex 3 at 298(2) K. The structures were solved by SHELXS-97 program (direct methods) and refined by Full-matrix least-squares on F^2 using SHELXL-97 program.

The thermogravimetry (TG), differential thermogravimetric (DTG), differential scanning calorimetric (DSC), and Fourier transform infrared (FTIR) analyses of the evolved gas of the title complexes were conducted using a TG/DSC-FTIR system, which was a Netzsch STA 449 F3 Instrument with a Bruker TENSOR 27 Fourier transform infrared spectrometer, under the simulated atmosphere (the gas flow rate of the nitrogen is 30 mL/min and the oxygen is 10 mL/min) with heat rate of 10K/min from 299.15 to 973.15K. About 5 mg sample was weighted into an open alumina crucible. The transfer line was used to link the Netzsch STA 449 F3 instrument and the heated gas cell of the FTIR instrument and both the transfer line and the gas cell were kept at a constant temperature of 473.15 K.

The heat capacities of the complexes were performed on a Netzsch DSC 200 F3 in the temperature range of 263.15 to 473.15 K under the linear heating rate of 10K/min using an indirect measurement method. The atmosphere was nitrogen gas, and the flow rate was 20 mL/min. The baseline, reference, and sample measurement were carried out under the same conditions. The sample mass were about 6 mg, and the reference standard substance sapphire mass used was 12.74 mg. The apparatus has an automatic data processing program from which we can obtain the C$_{p,m}$, curves of the sample by an indirect measurement method. Besides, four thermal circulating

3

processes for complexes 1 and 2 were measured by DSC in the temperature range of 263.15 to 473.15K under the scanning rate of 10 K/min. Furthermore, in order to study the phase transformation kinetics of complex 1, thermal circulating processes was measured by DSC under different scanning rates (7, 10, 12 and 15 K/min) in the temperature range of 263.15 to 473.15K.

Synthesis of [Ln(3,4,5-TEOBA)$_3$phen]$_2$ (Ln= La(1), Pr(2), Eu(3)). Two ligands of 3,4,5-TEOHBA (0.6mmol) and phen (0.2mmol) were dissolved in ethanol (95％) together, adjusting the pH of the solution to 6-7 with NaOH solution (1mol/L). Then the mixed ligands solution was added to the LnCl$_3$·H$_2$O (0.2mmol) aqueous solution under stirring. After stirring six hours and depositing twelve hours, the precipitates were filtered out and dried. After the volatilization of the mother liquor, single crystals of the title complexes were collected in two weeks at room temperature. Element alanalysis: calcd for complex 1: C, 56.77; H, 5.51; N, 2.60; La, 12.87. Found: C, 56.39; H, 5.57; N, 2.56; La, 13.05. Calcd for 2: C, 56.67; H, 5.50; N, 2.59; Pr, 13.04. Found: C, 56.26; H, 5.65; N, 2.53; Pr, 13.07; Calcd for 3: C, 56.09; H, 5.45; N, 2.57; Eu, 13.93. Found: C, 55.79; H, 5.45; N, 2.38; Eu, 14.22.

Results and Discussion

Molar conductance

Each complex was dissolved in DMSO with the concentration of 1×10^{-3} mol/L at room temperature. The values of molar conductance of complexes 1-3 are 8.72, 7.65, 7.35 S·cm^2·mol^{-1}, respectively, which implies three complexes are non-electrolyte. [28]

IR spectrum

The IR spectrum data of ligands and complexes are listed in Table 1. The similar IR spectrums of complexes indicate these three complexes are isostructural, [29] which is further proved by single crystal X-ray diffraction. Compared with the data of 3,4,5-TEOHBA, the characteristic absorption of $\nu_{C=O}$ (1686cm^{-1}) disappears, and $\nu_{sym(COO^-)}$ and $\nu_{asym(COO^-)}$ emerge at 1570-1576cm^{-1} and 1407-1425 cm^{-1}. [19, 30] The absorption of ν_{Ln-O} occurs in the vicinity of 417cm^{-1}, indicating that lanthanide ion is coordinated to the ligands. [31] The $\nu_{C=N}$ (1645cm^{-1}) and $\gamma_{=C-H}$ (864cm^{-1},738cm^{-1}) of phen are red shifted to $\nu_{C=N}$ (1609-1618cm^{-1}) and $\gamma_{=C-H}$ (843-848cm^{-1}, 730-733cm^{-1}), and this phenomenon also indicates the occurrence of coordination. [32]

Table 1

4

^{1}H, ^{13}CNMR spectra

Due to the paramagnetic properties and the low solubility of complexes 2 and 3, only the ^{1}H and ^{13}C NMR spectrum for ligands and complex 1 has been collected. The data are listed in Table 2.

The ^{1}H NMR spectrum data for ligands and complex 1 are shown in Table 2a. The ligand of 3,4,5-TEOHBA and 1,10-phen mainly show four chemical shifts, respectively. However, the chemical shift δ_H of (-COOH) disappears in the spectrum of complex 1, which indicates the ligand of 3,4,5-TEOHBA has coordinated to the lanthanide metal. And compared with the 3,4,5-TEOHBA ligand, chemical shift of the proton in benzene ring moves to high magnetic field, which attributes to the lower electro negativity of lanthanide metal than hydrogen atom. As a result, the electron cloud moves to benzene ring and tends to equilibration, all of which indicating that the chemical shift of the proton in benzene ring moves to high magnetic field for complex 1. [33] The chemical shift of δ_H for 1,10-phen almost has moved to low field after coordinating to the lanthanide metal, which attributes to the decrease of the density of electron cloud.

The ^{13}C NMR spectrum data for ligands and complex 1 in Table 2b show the chemical shift δ_C of (-COOH) move to low field, which indicates the group of (-COO) has coordinated to lanthanide metal. [34] Because of the increase of density of electron cloud, most δ_C in benzene ring and (-OCH$_2$CH$_3$) move to high field. For 1,10-phen, due to the coordination of nitrogen atoms and lanthanide metal, the density of electron cloud for phen ring has decreased, which makes δ_C moves to low field.

Table 2

Fluorescence spectrum

Photoluminescence properties of complex 3 in solid state have been investigated at room temperature. The excitation and emission spectra of complex 3 are shown in Figure 1. The photoluminescence spectra indicate typical Eu^{3+} luminescence as well as an antenna effect of the organic ligand. The excitation spectrum is recorded from 200 to 425 nm with the emission wavelength of 620nm. It reveals a prominent broad band from 200 to 370 nm, which can be assigned to the absorption of ligands. Other weaker signals at 395 and 465 nm can be assigned to direct Eu^{3+} excitation. [29] Complex 3 exhibits an intense characteristic red emission light under UV light. Emission spectrum of complex 3 shows four typical spectral bands of the europium complex

at 580, 593, 620 and 652 nm with excitation at 275 nm , which can be assigned to the characteristic f-f transitions from the emitting level $^5D_0$ to the ground multiplet ($^7F_0$, $^7F_1$,$^7F_2$ and $^7F_3$) of Eu(III) ion. Among them, Emission spectrum of complex 3 is dominated by the hypersensitive transition $^5D_0 \rightarrow ^7F_2$.

Fig. 1

Crystal Structure

Single crystals X-ray diffraction data of title complexes are given in Table 3. The selected bond lengths for complexes 1-3 are listed in Table 4. Single crystal X-ray crystallography analyses reveal that the title complexes are isostructurally crystallized in triclinic space group of P$\bar{1}$. The structure of complex 2 is described here representatively. As shown in Figure 2, complex 2 has two asymmetric structure units, and each unit has a nine coordinated center Pr^{3+} ion. Each Pr^{3+} ion is surrounded by one 1, 10-phen ligand and six 3, 4, 5-TEOBA ligands which adopt three different coordinated modes: bidentate chelating (O11, O12), bridging bidentate (O6, O7) and bridging tridentate (O1, O2 and O1#). Figure 3 shows that the nine coordinated Pr^{3+} can be described as a distorted monocapped square antiprism geometry, in which O1 acts as the capping atom. Two units are connected by two 3, 4, 5-TEOBA ligands adopting bridging tridentate coordinated mode and the distance of Pr-Pr bond is 4.044 Å. From Table 4, the distance of Pr-O bond is in the range from 2.40(2) to 2.706(15) Å and the average distance of Pr-O bond is 2.508 Å. Phen molecule bounds to the center metal adopting bidentate chelating mode. The average distance of Pr-N bond is 2.700 Å，which is longer than the distance of Pr-O bond. So, in the process of thermal decomposition, phen always tend to lose firstly. For the distance of Pr-O bond, due to the instability of the four member ring in bridging chelating, the length of Pr-O bond in bridging bidentate (2.447Å) is shorter than that in bidentate chelating(2.554 Å). [35] The binuclear molecular skeleton connect together to form a 1D chain via stacking π-π interactions between phen rings on neighboring complex molecules, which is shown in Figure 4. The attractive π-π interaction is formed by the centroid of phen in one binuclear molecular skeleton with the other centroid of phen in neighboring unit with the distance of 3.777 Å.

Fig. 2

Fig. 3

Fig. 4

6

Table 3

Table 4

Thermal behavior of title complexes

The TG, DTG and DSC curves of complexes 1-3 with the heating rate of 10 K/min from 299.15 to 973.15 K are shown in Figure 5. Stacked plots of the FTIR spectra of the evolved gas for complexes 1-3 are shown in Figure 6 and the data of thermal analysis for complexes 1-3 are given in Table 5. According to DSC analysis, the enthalpies and peak temperatures for three complexes are listed in Table 6.

Fig. 5

Fig. 6

Table 5

Table 6

Thermal decomposition of complexes 1-2 are similar and complex 1 will be described in detail. The thermal behavior of complex 1 is characterized by two stages with mass percent loss of 11.44% at 476.15-550.15K and 72.48% at 550.15-967.25K. In the first stage, there appears a small endothermic peak (T_p=494.85 K, $\triangle H_m$ =9.3803 KJ/mol) on DSC curve, which attribute to the release of part of phen molecule. However, corresponding to the Figure 6a, no signal is found in this temperature range. And this problem can be explained that the signal of gas is too weak so that the instrument can not detect. In Figure 6a, the strong signals are corresponding to the thermal decomposition of second stage. Figure 7 shows the IR spectrum of main gas products in different temperature of second stage. From 610.4K to 646.95K, the intensity of signal changes gradually and reaches to the maximum at 630.8K. The strongest signal from 2362 to 2312 cm^{-1} is corresponding to the absorption of CO_2. The absorption of CO and H_2O can be observed at 2114-2187cm^{-1} and 3503-3738cm^{-1}. Besides, some gaseous organics are detected in the FTIR spectra. The weak absorption at 1653 cm^{-1} is attributed to the $\nu_{C=N}$ from evolved phen, which can prove the decomposition of phen in second stage. The band from 2989 to 2941 cm^{-1} is considered as the ν_{C-H} from evolved aliphatic or aromatic hydrocarbons. At 1731 cm^{-1}, there is a characteristic peak which attribute to the $\nu_{C=O}$ of the carboxylic acid group, while the peak at 1211cm^{-1} are considered as the ν_{C-O} of the carboxylic acid group. The signals of 1510 and 1558 cm^{-1} are attributed to the $\nu_{C=C}$ of the benzene ring. [36] Above on, it can be concluded that the gaseous

products contain broken and not broken aromatic carboxylic ligands and part of phen ligands, which are detected in the form of gaseous small molecules (H_2O, CO_2 and CO) and molecule fragments of aromatic carboxylic ligands and phen ligands. In this stage, a strong exothermic peak can be observed on DSC curve (T_p=638.55 K, $\triangle H_m$ =-10334 KJ/mol). The general thermal decomposition reaction of complex 1 can be shown as follows:

$$[La(3,4,5\text{-}TEOBA)_3phen]_2 \xrightarrow[516.55K]{-xphen} La_2(3,4,5\text{-}TEOBA)_6phen_{(2-x)} + H_2O + CO_2 + \text{gaseous fragments}$$

$$La_2(3,4,5\text{-}TEOBA)_6phen_{(2-x)} \xrightarrow[632.15K]{-(2-x)phen\text{-}6(3,4,5\text{-}TEOBA)} La_2O_3 + H_2O + CO_2 + \text{gaseous fragments}$$
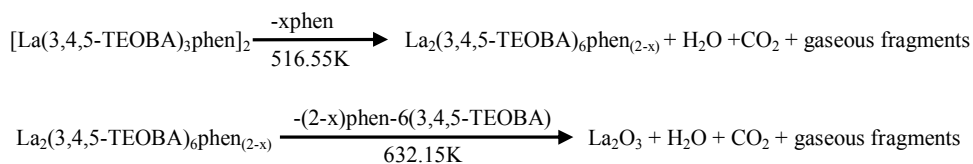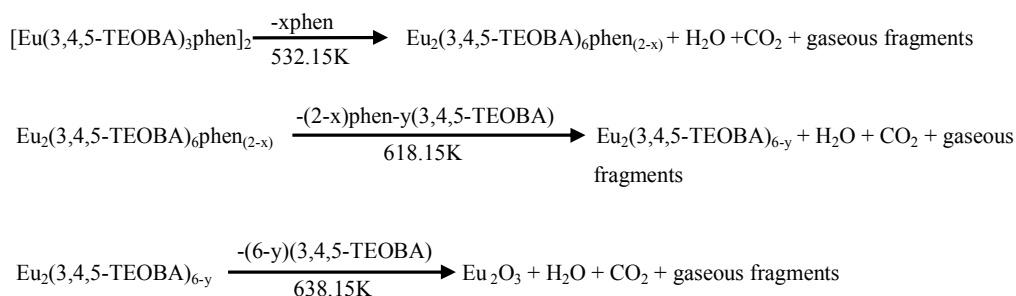
Fig. 7

From Figure 5c, the thermal decomposition of complex 3 is different from complexes 1-2 and it is characterized by three stages. Thermal decomposition of the first stage attribute to the release of part of phen molecules. However, as shown in Figure 6c, it is not detected in FTIR spectra and can be explained that the signal of gas is too weak. In second and third stages, the remainder phen and carboxylic ligands occur to decompose, which are same as the second stage for complex 1. However, the characteristic absorption of only one stage was found in FTIR spectra. The reactions of second and three stages occur continuously, so that only one set of signal is detected by instrument. The general thermal decomposition reaction of complex 3 can be shown as follows:

$$[Eu(3,4,5\text{-}TEOBA)_3phen]_2 \xrightarrow[532.15K]{-xphen} Eu_2(3,4,5\text{-}TEOBA)_6phen_{(2-x)} + H_2O + CO_2 + \text{gaseous fragments}$$

$$Eu_2(3,4,5\text{-}TEOBA)_6phen_{(2-x)} \xrightarrow[618.15K]{-(2-x)phen\text{-}y(3,4,5\text{-}TEOBA)} Eu_2(3,4,5\text{-}TEOBA)_{6-y} + H_2O + CO_2 + \text{gaseous fragments}$$

$$Eu_2(3,4,5\text{-}TEOBA)_{6-y} \xrightarrow[638.15K]{-(6-y)(3,4,5\text{-}TEOBA)} Eu_2O_3 + H_2O + CO_2 + \text{gaseous fragments}$$

Heat capacities

Based on the TG-DTG/DSC curve, there is no mass loss before 463.15K for three complexes. So the heat capacities of the title complexes have been measured by DSC in the temperature range from 263.15 to 463.15 K. The values of average molar heat capacities for title complexes are listed in Table S1 and plotted in Figure 8. The values of experimental heat capacities are fitted to the

polynomial equations by means of least square method in the reduced temperature (x) and obtained correlation coefficient (R^2) and standard deviation (SD). The reduced temperature is calculated by the equation of x=[T-(T_{max}+T_{min})/2]/[(T_{max}-T_{min})/2], T is the experimental temperature, T_{max} and T_{min} are the upper limit and down limit, respectively. [37, 38] As shown in Figure 9a, during 280-350K, there is a peak for complexes 1-3, respectively, which can be proved to be solid-to-solid phase transition by thermal circulating processes. [24, 36, 39] The curves of complexes 1-2 are fitted in three phases in which the phase transition peaks are also fitted. The peak of solid-to-solid phase transition for complex 3 is weaker and the curve of complex 3 is fitted in two phases. The results are shown in Scheme 1.

Fig. 8

Scheme 1

Based on the fitted polynomial and thermodynamic equations, the smoothed heat capacities and thermodynamic functions of the three complexes are calculated. The thermodynamic equations are as follows:

$$H_T - H_{298.15} = \int_{298.15}^{T} C_{P,m} dT$$

$$S_T - S_{298.15} = \int_{298.15}^{T} C_{p,m} T^{-1} dT$$

$$G_T - G_{298.15} = \int_{298.15}^{T} C_{p,m} dT - T \int_{298.15}^{T} C_{P,m} T^{-1} dT$$

The smoothed values of $C_{p,m}$ and thermodynamic functions relative to the standard reference temperature 298.15 K with an interval of 10 K are shown in Table S2.

Thermal circulating and phase transformation kinetics

Four thermal circulating processes have been designed for complexes 1 and 2 with the scanning rate of 10 K/min from 263.15-463.15K and the DSC curves of thermal circulating are shown in Figure 9. The temperature and enthalpy of endothermic and exothermic in every process for complexes 1 and 2 is listed in Table 7. As a result, the reversibility and repeatability of the phase transitions of the sample are verified. There is almost no change in peak position of each circulating process, which can preferably explain the presence of solid to solid phase transition. As shown in Table 7, in the same circulating process, the phase transition temperature in cooling process is lower than that in heating process, which means supercooling phenomenon occurs in the thermal circulating processes of complexes 1 and 2. The values of enthalpy in heating and

9

cooling processes for complexes 1 and 2 are decreased gradually. For example, the value of enthalpy for complex 1 is 8.414 KJ/mol at the first heating circulation and with the continuing of the circulation, the value of enthalpy decrease to 7.488 KJ/mol gradually at last heating circulation. However, there is no endothermic peak before 473.15K in Figure 5, which probably attributed to the highly sensitivity of the instrument of DSC 200 F3.

Fig. 9

Table 7

The enthalpy of heating processes for complex 1 is larger than others, so the accuracy of measurement is higher. Only the heating processes of complex 1 have been studied in phase transformation kinetics. The activation energy (E) of four circulating processes for complex 1 is calculated by the iso-conversional method: M. J. Starink [40] and Madhusudanan-Krishnan-Ninan [41]. The equations are as follows:

M. J. Starink:

$$\ln\left(\frac{\beta}{T^{1.92}}\right) = C - 1.0008\frac{E}{RT} \tag{1}$$

Madhusudanan-Krishnan-Ninan:

$$\ln\left[\frac{G(\alpha)}{T^{1.921503}}\right] = \left[\ln\frac{AE}{\beta R} + 3.772050 - 1.921503\ln E\right] - 0.120394(E/T) \tag{2}$$

Equation (2) can be changed into:

$$\ln\left[\frac{\beta}{T^{1.921503}}\right] = \left[\ln\frac{AE}{G(\alpha)R} + 3.772050 - 1.921503\ln E\right] - 0.120394(E/T) \tag{3}$$

The relationship of activation energy (E) and percent conversion (α) for different circulating processes with two methods are displayed in Figure 10. As shown in Figure 10, the values of activation energy (E) in different percent conversion calculated by two methods are almost unanimous and in four circulations activation energy (E) and percent conversion (α) exhibit the fine linear relationship. The curves in Figure 10 are linear fitted and the equations are listed in Table 8. The activation energy (E) of the first circulation is deviated from the other circulation, which may be attributed to the uncertainty of initial waiting for DSC.

Fig. 10

Table 8

Conclusions

In summary, we reported the synthesis and characterization of the title complexes. Three complexes are isostructural and they are all binuclear molecules. The neighboring complex molecules are connected together to form a 1D chain via stacking π-π interactions. Complex [Eu(3,4,5-TEOBA)$_3$phen]$_2$ shows the characteristic emission of Eu^{3+}. According to the study on thermal decomposition data and stacked plots of the FTIR spectra of the evolved gas, we have obtained the thermal decomposition mechanism of the title complexes. The heat capacities of complexes show that there is a solid-to-solid phase transition for each complex. The thermal circulating of solid-to-solid phase transition for complexes 1and 2 have been measured, and phase transformation kinetics of complex 1 have been studied. The results show the activation energy (E) and the percent conversion (α) display the linear relationship.

Acknowledgments

Electronic Supplementary Information (ESI) available: Experimental molar heat capacities of complexes 1-3. Smoothed molar heat capacities and thermodynamic functions of complexes 1-3. The numbers of the three complexes (CCDC 1024382 (1), 1023816 (2), 1023820 (3)) contain the supplementary crystallographic data for this paper, which can be obtained free of charge from the Cambridge Crystallographic Data Centre via www.ccdc.cam.ac.uk/data_request/cif.

Reference

1. A. O. Borodin, G. A. Kostin, P. E. Plusnin, E. Y. Filatov, A. S. Bogomyakov and N. V. Kuratieva, *Eur. J. Inorg. Chem.*, 2012, 2298.

2. L. De Almeida, S. Grandjean, N. Vigier and F. Patisson, *Eur. J. Inorg. Chem.*, 2012, 4986.

3. R. Łyszczek, *J. Therm. Anal. Calorim.*, 2011, **108**, 1101.

4. R. Y. Wang, M. Liu, C. Zhao, G. F. Liu, X. Zhu and Y. Yang, *J. Inorg. Organomet. Polym.*, 2013, **24**, 442.

5. S. V. Eliseeva, M. Ryazanov, F. Gumy, S. I. Troyanov, L. S. Lepnev, J. C. G. Bünzli and N. P. Kuzmina, *Eur. J. Inorg. Chem.*, 2006, 4809.

6.   S. J. Makowski, A. Schwarze, P. J. Schmidt and W. Schnick, *Eur. J. Inorg. Chem.*, 2012, 1832.

7.   M. Paluch, P. Gawryszewska, T. Lis and J. Lisowski, *Polyhedron*, 2010, **29**, 3387.

8.   X. Feng, X. L. Ling, B. Liu, Z. Q. Shi, J. J. Shang and L. Y. Wang, *Inorg. Chem. Commun.*, 2012, **20**, 1.

9.   E. R. Souza, I. O. Mazali and F. A. Sigoli, *J. Fluoresc.*, 2014, **24**, 203.

10.   Z. Rzączyńska, A. Kula, J. Sienkiewicz-Gromiuk and A. Szybiak, *J. Therm. Anal. Calorim.*, 2011, **103**, 275.

11.   E. Debroye, M. Ceulemans, L. Vander Elst, S. Laurent, R. N. Muller and T. N. Parac-Vogt, *Inorg. Chem.*, 2014, **53**, 1257.

12.   Y. F. Yuan, T. Cardinaels, K. Lunstroot, K. V. Hecke, L. V. Meervelt, C. Gorller-Walrand, K. Binnemans and P. Nockemann, *Inorg. Chem.*, 2007, **46**, 5302.

13.   W. Ahmad, L. J. Zhang and Y. S. Zhou, *CrystEngComm*, 2014, **16**, 3521.

14.   J. Garcia-Torres, P. Bosch-Jimenez, E. Torralba-Calleja, M. Kennedy, H. Ahmed, J. Doran, D. Gutierrez-Tauste, L. Bautista and M. Della Pirriera, *J. Photoch. Photobio. A*, 2014, **283**, 8.

15.   A. R. Ramya, D. Sharma, S. Natarajan and M. L. Reddy, *Inorg. Chem.*, 2012, 51, 8818.

16.   H. B. Zhang, L.J. Zhou, J. Wei, Z. H. Li, P. Lin and S. W. Du, *J.Mater.Chem.*, 2012, **22**, 21210.

17.   Y. S. Zhou, X. M. Li, L. J. Zhang, Y. Guo and Z. H. Shi, *Inorg. Chem.*, 2014, **53**, 3362.

18.   K. P. Carter, S. J. A. Pope and C. L. Cahill, *CrystEngComm*, 2014, **16**, 1873.

19.   X. Zhao, X. Y. Yu, T. L. Chen, Y. H. Luo, J. J. Yang and H. Zhang, *Inorg. Chem. Commun.*, 2012, **20**, 247.

20.   K. Chen, Z. G. Sun, Y. Y. Zhu, Z. M. Liu, F. Tong, D. P. Dong, J. Li, C. Q. Jiao, C. Li and C. L. Wang, *Cryst. Growth. Des.*, 2011, **11**, 4623.

21.   Y. X. Chi, Y. J. Liu, Y. Li, R. Wang, J. Jin, G. N. Zhang and S. Y. Niu, *J. Mol. Struct.*, 2012, **1018**, 122.

22.   W. X. Li, F. Guo, Y. S. Zheng, X. F. Cao, S. Y. Feng, J. Bai and X. D. Xin, *J. Lumin.*, 2014, **153**, 421.

23.   E. Kusrini, M. I. Saleh and A. Usman, *J. Chem. Crystallogr.*, 2010, 41, 87.

24.   K. Tang, H. M. Liu, N. Ren, J. J. Zhang and K. Z. Wu, *J. Chem. Thermodyn.*, 2012, **47**, 428.

25.   Y. X. Chi, J. Q. Qiu, W. T. Zhu, J. Jin, S. Y. Niu and G. N. Zhang, *J. Inorg. Organomet. P*,

2011, **22**, 125.

26. R. Yuan, C. Chen and N. Zhang, *J. Inorg. Organomet. P*, 2012, **22**, 507.

27. Y. E. Cha, X. Li, D. Ma and R. Huo, *Eur. J. Inorg. Chem.*, 2014, 2969.

28. W. J. Geary, *Coordin. Chem. Rev.*, 1971, **7**, 81.

29. L. F. Marques, A. A. B. C. Junior, C. C. Correa, M. G. Lahoud, R. R. da Silva, S. J. L. Ribeiro and F. C. Machado, *J. Photoch. Photobio A*, 2013, **252**, 69.

30. J. R. Zheng, N. Ren, J. J. Zhang, D. H. Zhang, L. Z. Yan and Y. Li, *J. Chem. Eng. Data*, 2012, **57**, 2503.

31. J. J. Liu, N. Ren, J. J. Zhang, C. Y. Zhang and H. H. Song, *Sci. China Chem.*, 2014, **57**, 1520.

32. J. Y. Liu, N. Ren, J. J. Zhang, S. M. He and S. P. Wang, *Ind. Eng. Chem. Res*, 2013, **52**, 6156.

33. L. Tian, N. Ren, J. J. Zhang, H. M. Liu, J. H. Bai, H. M. Ye and S. J. Sun, *Inorg. Chim. Acta*, 2009, **362**, 3388.

34. Q. Q. Yang, L. S. Li and Z. J. Zhu, *Chinese J. Magn. Reson.*(in Chinese), 1997, **14**, 533.

35. J. F. Wang, H. Li, J. J. Zhang, N. Ren and K. Z. Wu, *Sci. China. Chem*, 2012, **55**, 2161.

36. S. Jingyan, L. Jie, D. Yun, H. Ling, Y. Xi, W. Zhiyong, L. Yuwen and W. Cunxin, *J. Therm. Anal. Calorim*, 2008, **93**, 403.

37. J. P. Guo, B. P. Liu, X. C. Lv, Z. C. Tan, B. Tong, Q. Shi and D. F. Wang, *J. Chem. Eng. Data*, 2007, **52**, 1678.

38. M. H. Wang, Z. C. Tan, X. H. Sun,[25] H. T. Zhang, B. P. Liu, L. X. Sun and T. Zhang, *J. Chem. Eng. Data*, 2005, **50**, 270.

39. D. f. Lu, Y. y. Di and J. m. Dou, *Sol. Energ. Mat. Sol. C.*, 2013, **114**, 1.

40. M. J. Starink, *Thermochim. Acta*, 2003, **404**, 163.

41. P. M. Madhusudanan, K. Krishnan and K. N. Ninan, *Thermochim. Acta*, 1986, **97**, 189.

Table 1 Frequencies (cm^{-1}) of the absorption bands for the ligands and title complexes

Ligand/ complex	$\nu_{C=N}$	$\gamma_{=C-H}$	$\nu_{C=O}$	$\nu_{sym(COO^-)}$	$\nu_{asym(COO^-)}$	ν_{Ln-O}
phen	1645	864, 738				
3,4,5-TEOHBA			1686			
1	1618	843, 731		1570	1410	417
2	1609	848, 730		1576	1407	417
3	1618	848, 733		1576	1425	419

Table 2a ^{1}H NMR spectra data of ligands and complex1.
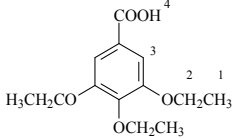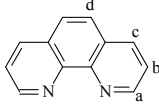
Ligands and complex	^{1}H NMR (δ /ppm)							
	δ_1	δ_2	δ_3	δ_4	δ_a	δ_b	δ_c	δ_d
(COOH structure, 3,4,5-triethoxybenzoic acid)	1.34	4.06	7.20	12.87				
[La(3,4,5-TEOBA)$_3$phen]$_2$	1.28	4.02	7.17					
(phen structure)					9.11	7.76	8.48	7.97
[La(3,4,5-TEOBA)$_3$phen]$_2$					9.13	7.80	8.52	8.02

Table 2b ^{13}C NMR spectra data of ligands and complex1.
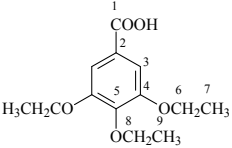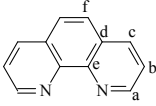
Ligands and complex	^{13}C NMR (δ /ppm)								
(COOH structure)	δ_1	δ_2	δ_3	δ_4	δ_5	δ_6	δ_7	δ_8	δ_9
	167.45	126.11	107.99	152.63	141.41	64.56	15.14	68.50	15.89
[La(3,4,5-TEOBA)$_3$phen]$_2$	176.49	127.18	107.60	152.10	139.84	64.30	15.22	68.27	15.91
(phen structure)	δ_a	δ_b	δ_c	δ_d	δ_e	δ_f			
	150.41	123.76	136.65	128.92	146.03	127.13			
[La(3,4,5-TEOBA)$_3$phen]$_2$	150.53	123.86	136.85	128.98	145.93	127.18			

14

Table 3 Crystal data and structure refinement of the title complexes

Complex	1	2	3
Empirical formula	$C_{102} H_{118} La_2 N_4 O_{30}$	$C_{102} H_{118} Pr_2 N_4 O_{30}$	$C_{102} H_{118} Eu_2 N_4 O_{30}$
Formula weight	2157.82	2161.82	2183.92
Temperature/K	298(2)	298(2)	298(2)
Wavelength/Å	1.54178	1.54178	0.71073
Crystal system,	Triclinic,	Triclinic,	Triclinic,
space group	P$\bar{1}$	P$\bar{1}$	P$\bar{1}$
Unit cell dimensions			
a/ Å	13.0256(13)	12.9555(12)	12.7320(11)
b/ Å	14.4709(12)	14.4344(13)	14.3480(12)
c/ Å	15.0513(15)	15.077(2)	15.0480(14)
α/deg	84.356(7)	84.255(9)	83.4850(10)
β/deg	73.226(9)	73.642(10)	75.328(2)
γ/deg	89.335(7)	89.269(7)	89.450(2)
Volume/ Å^3	2702.8(4)	2691.4(5)	2641.6(4)
Z, Calculated density/(Mg/m^3)	1, 1.326	1, 1.334	1, 1.373
Absorption coefficient/mm^{-1}	6.647	7.485	1.253
$F(000)$	1112	1116	1124
Crystal size/ mm	0.19 x 0.17 x 0.16	0.27 x 0.09 x 0.05	0.35 x 0.10 x 0.07
θ range for data collection/ deg.	3.07 to 66.05	3.07 to 66.05	2.72 to 25.02
Limiting indices	-15≤h≤15,	-15≤h≤15,	-15≤h≤15,
	-17≤k≤9,	-17≤k≤17,	-17≤k≤11,
	-17≤l≤17	-9≤l≤17	-17≤l≤17
Reflections collected / unique	17460 / 9395	9359 / 9359	13550 / 9166
	[$R_{(int)}$ = 0.0890]	[$R_{(int)}$ = 0.0000]	[$R_{(int)}$ = 0.0661]
Completeness to θ = 66.05	99.7 %	99.8 %	
Completeness to θ = 25.02			98.3 %
Max. and min. transmission	0.4160 and 0.3648	0.7060 and 0.2371	0.9174 and 0.6682
Data / restraints / parameters	9395 / 1 / 632	9359 / 0 / 632	9166 / 1 / 631
Goodness-of-fit on F^2	1.039	1.099	1.024
Final R indices [$I>2\sigma(I)$]	R_1 = 0.1273,	R_1 = 0.1423,	R_1 = 0.1005,
	wR_2 = 0.3180	wR_2 = 0.3553	wR_2 = 0.2479
R indices (all data)	R_1 = 0.1797,	R_1 = 0.2628,	R_1 = 0.1684,
	wR_2 = 0.3739	wR_2 = 0.4404	wR_2 = 0.2903
Largest diff. peak and hole/(e.A^{-3})	1.433 and -1.091	0.905 and -1.045	1.298 and -1.140

15

Table 4 Selected bond lengths (Å) of the title complexes

Complex 1			
La(1)-O(6)	2.427(8)	La(1)-O(12)	2.563(8)
La(1)-O(1)#1	2.475(7)	La(1)-N(2)	2.709(9)
La(1)-O(7)#1	2.494(8)	La(1)-O(1)	2.737(6)
La(1)-O(2)	2.542(9)	La(1)-N(1)	2.745(9)
La(1)-O(11)	2.553(8)	La(1)-La(1)#1	4.0900(10)
Complex 2			
Pr(1)-O(6)	2.40(2)	Pr(1)-O(11)	2.520(16)
Pr(1)-O(1)#1	2.455(18)	Pr(1)-N(2)	2.69(2)
Pr(1)-O(2)	2.480(18)	Pr(1)-O(1)	2.706(15)
Pr(1)-O(7)#1	2.485(17)	Pr(1)-N(1)	2.71(2)
Pr(1)-O(12)	2.510(17)	Pr(1)-Pr(1)#1	4.044(2)
Complex 3			
Eu(1)-O(1)#1	2.353(10)	Eu(1)-O(12)	2.449(10)
Eu(1)-O(6)	2.360(11)	Eu(1)-N(2)	2.575(14)
Eu(1)-O(7)#1	2.377(9)	Eu(1)-N(1)	2.642(13)
Eu(1)-O(2)	2.442(9)	Eu(1)-O(1)	2.706(9)
Eu(1)-O(11)	2.449(9)	Eu(1)-Eu(1)#1	3.9746(13)

Symmetry transformations used to generate equivalent atoms:

#1 -x+1,-y+1,-z+1

Table 5 Thermal decomposition data of the title complexes (β=10 K/min)

Complex	Stage	Temperature range/K	DTG T_p /K	Mass loss rate/% found	Mass loss rate/% calcd	Probable removed groups	Intermediate and final solid products
	I	476.15-550.15	516.55	11.44		xphen	La$_2$(3,4,5-TEOBA)$_6$
1							phen$_{(2-x)}$
	II	550.15-967.25	632.15	72.48		(2-x)phen+6(3,4,5-TEOBA)-3O	La$_2$O$_3$
				83.92	84.93[a]		
2	I	485.15-563.15	515.85	4.48		xphen	Pr$_2$(3,4,5-TEOBA)$_6$
							phen$_{(2-x)}$
	II	563.15-967.45	622.15	77.67		(2-x)phen+6(3,4,5-TEOBA) -11/3O	11/3Pr$_6$O$_{11}$
				82.15	84.24[a]		
3	I	493.15-583.15	532.75	14.12		xphen	Eu$_2$(3,4,5-TEOBA)$_6$
							phen$_{(2-x)}$
	II	583.15-627.15	618.15	40.73		(2-x)phen+y(3,4,5-TEOBA)	Eu$_2$(3,4,5-TEOBA)(6-y)
	III	627.15-967.25	638.15	27.28		(6-y)(3,4,5-TEOBA)-3O	Eu$_2$O$_3$
				82.13	83.88[a]		

T_p is the peak temperature of DTG

[a]The total loss rate.

16

Table 6 Enthalpies and peak temperatures for the title complexes from DSC analysis of TG/DSC-FTIR system.

Complex	Stage	Temperature rage (K)	DSC peak Temperature (K)	$\triangle H_m$ (KJ/mol)
1	I	492.25-497.15	494.85	9.3803
	II	629.45-645.65	638.55	-10334
2	I	510.05-516.15	512.35	6.0166
	II	620.25-642.75	634.85	-13380
3	I	509.25-519.25	514.25	30.575
	II	616.05-626.85	620.65	-1422.0
	III	632.85-649.85	642.95	-15231

Table 7 Enthalpies and peak temperatures for complexes 1 and 2 in four circulating processes.

complexes		heating				cooling			
	step	$T_0(K)$	$T_t(K)$	$T_p(K)$	Endothermic (KJ/mol)	$T_0(K)$	$T_t(K)$	$T_p(K)$	Exothermic (KJ/mol)
	1	324.52	329.29	326.62	8.414	293.45	302.87	298.70	-5.936
1	2	324.46	329.15	326.61	8.114	293.38	302.68	298.83	-5.703
	3	324.39	329.19	326.53	7.779	293.47	302.83	298.66	-5.604
	4	324.38	329.19	326.51	7.488	293.29	302.84	298.44	-5.336
	1	312.70	323.67	318.02	5.483	278.82	288.92	283.45	-1.668
2	2	312.64	323.40	317.8	5.476	280.09	288.84	282.50	-1.492
	3	312.94	323.93	317.72	5.433	277.94	288.68	283.37	-0.871
	4	312.58	323.63	317.48	5.243	277.71	288.53	282.90	-0.855

T_0 is the initial temperature of the phase transition peak by DSC extrapolation;

T_t is the ending temperature of the phase transition peak by DSC extrapolation;

T_p is the peak temperature of the phase transition peak.

Table 8 The linear fitting results of E and α of the heating processes for complex 1.

M. J. Starink

Circulation process	Equation	R	SD
1	E=439.29087-212.28831α	-0.99716	4.08506
2	E=380.61997-169.18766α	-0.99176	5.56670
3	E=379.85463-168.48214α	-0.98944	6.28491
4	E=373.61061-162.53506α	-0.98642	6.89242

Madhusudanan-Krishnan-Ninan

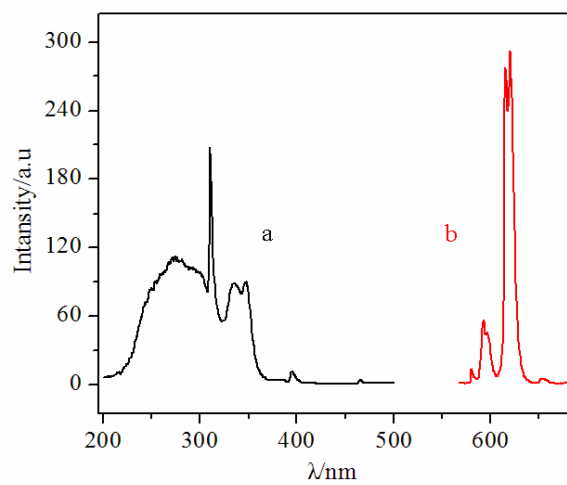| Circulation process	Equation	R	SD
1	E=439.21608-212.25162α	-0.99716	4.08456
2	E=380.55899-169.16656α	-0.99175	5.56668
3	E=379.79702-168.46039α	-0.98944	6.28456
4	E=373.55174-162.51526α	-0.98642	6.89120

Fig. 1 Excitation spectra (a) with the emission wavelength of 620 nm and emission spectra (b)
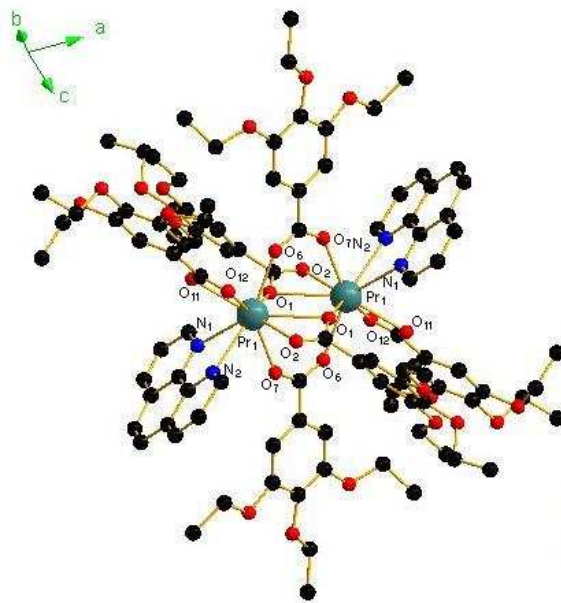
with excitation at 275 nm for complex 3.

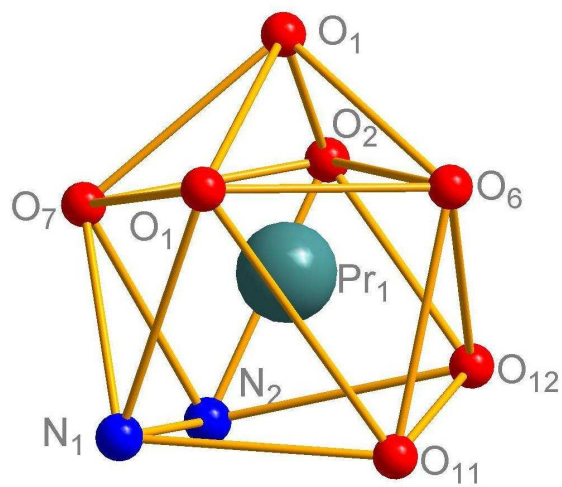**Fig. 2** Crystal structure of the complex 2.

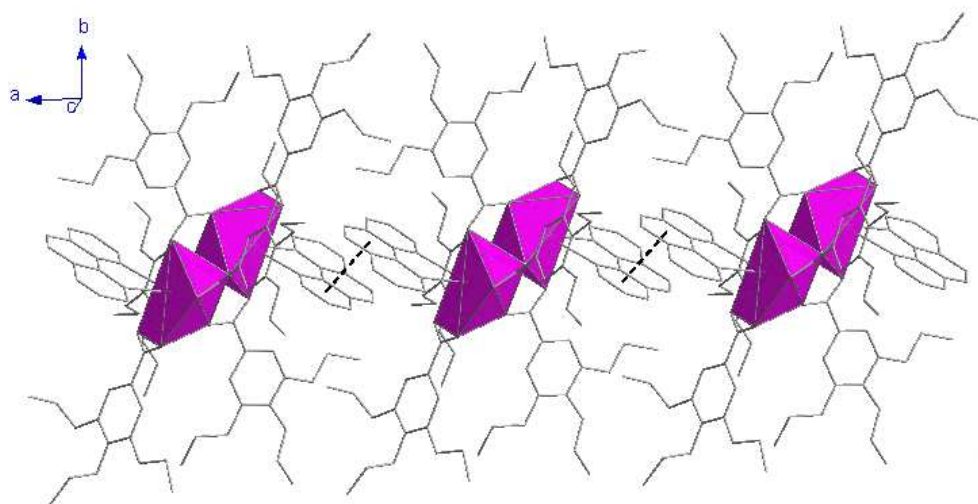**Fig. 3** Coordination geometry of Pr^{3+} ion

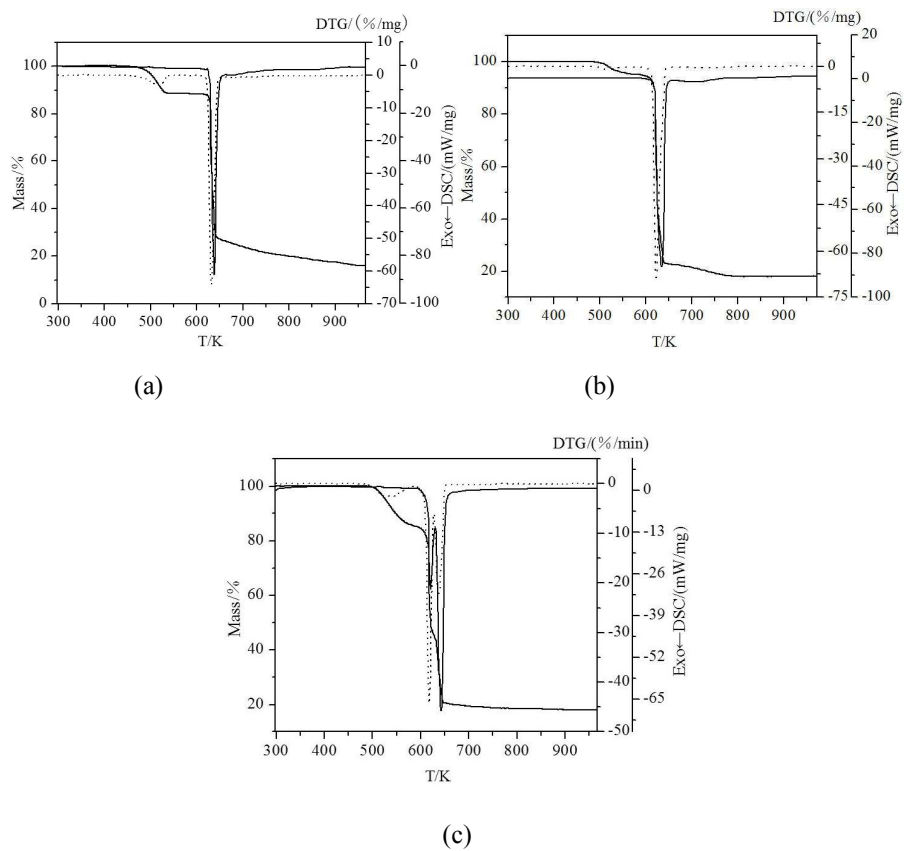**Fig. 4** Binuclear units of complex 2 are stitched together via stacking π-π interactions to form 1D

chain.

Fig. 5 TG-DTG/DSC curves of complexes 1-3 at the heating rate of 10 K/min
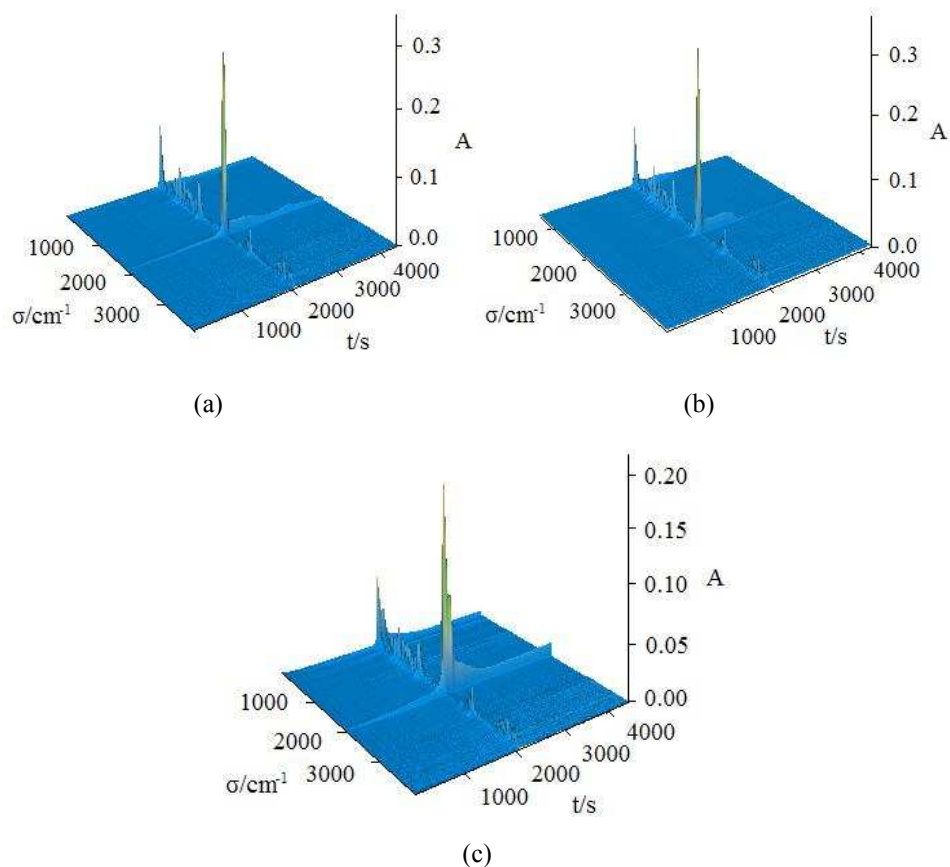
(complex1=a, complex 2=b, complex3=c).

(a)

(b)

(c)

Fig. 6 Stacked plots of the FTIR spectra of the evolved gases for complexes 1-3 as observed in the

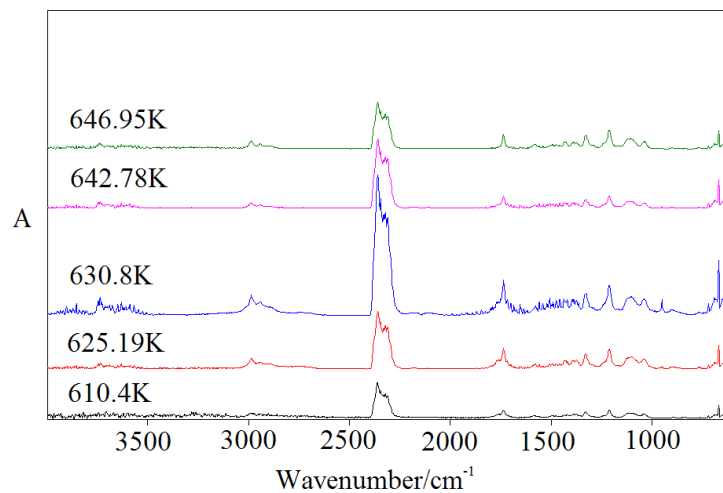online TG/DSC-FTIR system at the heating rate of 10 K/min (complex1=a, complex 2=b,

complex3=c).

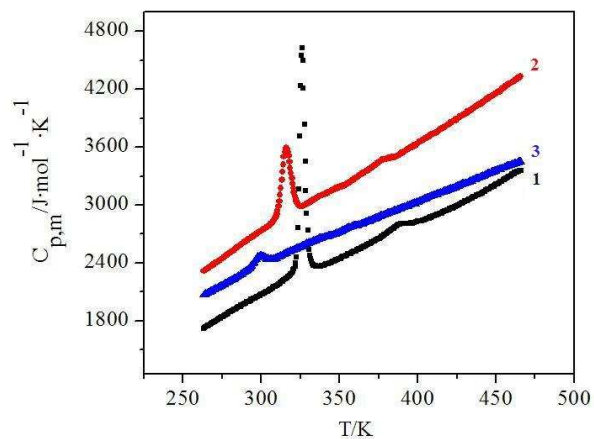**Fig. 7** FTIR spectra of the evolved gases for complex 1 at different temperature.

21

Fig. 8 Relationship of molar heat capacities varying with temperature
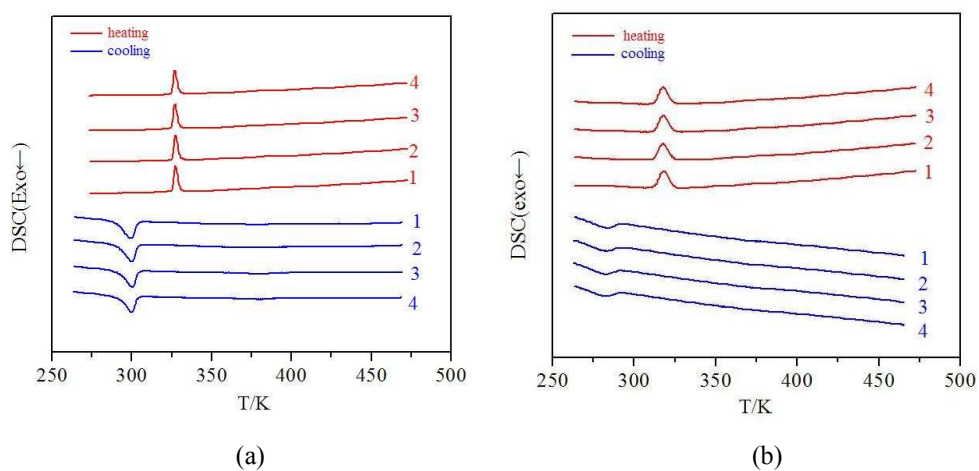
(Lines 1-3 represent complexes 1-3, respectively).

| (a) | (b) |

Fig. 9 The DSC curves of the complexes 1 (a) and 2 (b) in the four circulating processes.
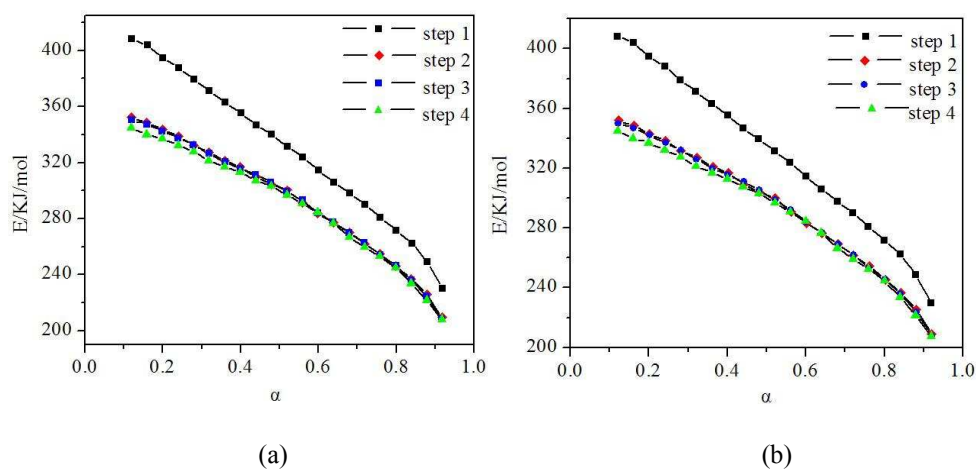

| (a) | (b) |

Fig. 10 The relationship of activation energy (E) and percent conversion (α) of the heating

processes for complex 1. (M. J. Starink (a); Madhusudanan-Krishnan-Ninan (b))

Complex 1 [La(3,4,5-TEOBA)$_3$phen]$_2$

T=263.15K-317.65K

$C_{p,m}$/J·K^{-1}·mol^{-1}=1986.47349+240.21126x-39.39713x^2-44.02844x^3+82.91937x^4-62.41169x^5

$\qquad$ -70.10217x^6+81.48358x^7+30.65699x^8-34.90114x^9

$\qquad\qquad$ R^2=0.9993 SD=1.27517

T=318.15K-338.15K

$C_{p,m}$/J·K^{-1}·mol^{-1}=3689.28935-6388.81941x-6372.03235x^2+49253x^3+8605.0277x^4-130626.0704x^5

$\qquad$ -2273.54941x^6+143629.30408x^7-1372.40494x^8-55876.49448x^9

$\qquad\qquad$ R^2=0.96383 SD=156.00023

T=338.65K-466.15K

$C_{p,m}$/J·K^{-1}·mol^{-1}=2845.82158+260.17669x+59.78089x^2+1530.63056x^3-494.07487x^4

$\qquad$ -3962.13963x^5+943.83048x^6+4522.5055x^7-493.09449x^8-1859.32682x^9

$\qquad\qquad$ R^2=0.9995 SD=6.39257

Complex 2 [Pr(3,4,5-TEOBA)$_3$phen]$_2$

T=263.15K-306.15K

$C_{p,m}$/J·K^{-1}·mol^{-1}= 2557.68661+250.36888x-14.09125x^2-6.25456x^3+36.34039x^4-2.67192x^5

$\qquad$ -62.59258x^6-34.30214x^7+37.03968x^8+37.69702x^9

$\qquad\qquad$ R^2=0.99981 SD=2.08584

T=306.65K-326.15K:

$C_{p,m}$/J·mol^{-1}·K^{-1}=3578.89209-166.33847x-3515.89891x^2+2167.51795x^3+7574.60393x^4

$\qquad$ -5933.09602x^5-7544.93273x^6+6577.77093x^7+2806.92874x^8-2558.05762x^9

$\qquad\qquad$ R^2=0.9993 SD=7.56407

T=326.65K-465.65K:

$C_{p,m}$/J·mol^{-1}·K^{-1}=3601.50052+597.87955x+240.59965x^2+440.70301x^3-960.63864x^4

$\qquad$ -934.65648x^5+1587.47986x^6+754.29082x^7-823.20267x^8-184.52948x^9

$\qquad\qquad$ R^2=0.99968 SD=6.99494

Complex 3 [Eu(3,4,5-TEOBA)$_3$phen]$_2$

T=263.15K-279.65K

$$C_{p,m}/\text{J}\cdot\text{mol}^{-1}\cdot\text{K}^{-1}=2135.67828+60.95561x-23.68713x^2+94.64313x^3+102.18901x^4-262.13515x^5$$

$$-141.36456x^6+288.39681x^7+64.74469x^8-110.98893x^9$$

$$R^2=0.99884 \quad SD=1.72051$$

T=280.15K-309.65K

$$C_{p,m}/\text{J}\cdot\text{mol}^{-1}\cdot\text{K}^{-1}=2395.72372+331.91648x-13.53427x^2-1051.26934x^3-555.14935x^4$$

$$+2051.47772x^5+962.47884x^6-1817.56269x^7-463.51602x^8+601.89807x^9$$

$$R^2=0.99909 \quad SD=2.89166$$

Scheme 1 The fitting results of the experimental heat capacities in the reduced temperature by means of the least-squares method.